The Energized Point Process as a Model for Wirelessly Powered Communication Networks

Na Deng, *Member, IEEE*, and Martin Haenggi, *Fellow, IEEE*

***Abstract*—The spatial correlation of the RF-powered nodes that harvest enough energy plays a critical role in the performance evaluation of large-scale wirelessly powered communication networks (WPCNs). However, such correlation is mostly ignored in the literature for analytical tractability. In this paper, we explore the correlation and propose a new point process, named *energized point process* (EPP), as a model for the RF-powered nodes that succeed in harvesting energy. Specifically, we focus on the spatial correlation of the energy harvested from a Poisson field of RF power sources. Two energy harvesting models with different degrees of practicality are introduced to concretize the EPP with the aim of visualizing the point process of the energized nodes and characterizing its density and pair correlation function theoretically. It turns out that for both models the resulting process exhibits positive correlation. With the first- and second-order statistics of the EPP, we use a fitted Poisson cluster process to provide good approximations of the success probability and area spectral efficiency in the information transmission phase. Numerical results investigate the impacts of the key parameters related to the energy transfer on the spatial correlation of the EPP and the communication performance. An important conclusion is that although the Poisson point process has been so far the most widely used model for wirelessly powered networks, it is inadequate due to the positive energy correlation.**

***Index Terms*—Energy correlation; wirelessly powered communication networks; wireless energy transfer; Poisson cluster process; stochastic geometry.**

I. Introduction

A. Motivation

As a new enabler for energy harvesting, wireless energy transfer (WET) is anticipated to have important applications in future energy-constrained wireless communication networks [2]. This integration of RF-based energy harvesting in communication networks renders the spatial structure of transmitters (including the RF sources and the RF-powered nodes) even more crucial since it not only determines the mutual interference and the signal-interference-plus-noise ratio (SINR) performance in conventional communications but also the energy that can be harvested. As a consequence, stochastic geometry models for wirelessly powered communication networks (WPCNs) have recently received widespread attention due to their capability of capturing the irregularity and variability of the node configurations in real networks and providing theoretical insights [3–6].

The Poisson point process (PPP) has been by far the most popular spatial model for various types of wireless networks []. This is because the PPP model has several convenient features, such as the independence between points and the simple form of the probability generating functional (PGFL) [7]. Therefore, the PPP model of RF transmitters permits a tractable analysis for the energy outage probability [3] as well as the energy meta distribution in the energy harvesting phase [8]. As for the information transmission phase, the analysis in previous works is mostly based on the assumption that the active RF-powered nodes, which are the nodes that successfully harvest energy from a Poisson field of RF transmitters, are formed by independently thinning the Poisson distributed RF-powered nodes [5, 6, 8]. Hence, the active RF-powered nodes are assumed to also form a PPP. However, this does not seem realistic since if a node succeeds in harvesting energy, a nearby node will have a good chance of succeeding also, and vice versa. In other words, the nodes that successfully harvest energy from a Poisson field of transmitters are not mutually independent but *spatially correlated*. Therefore, it is important to fully characterize the spatial correlation of the energy harvested from RF transmitters and the corresponding effect on the performance of communication systems, which, to our best knowledge, have not been studied in large-scale settings previously.

B. Related Work

For WPCNs, the downlink wireless information and energy transfer has been extensively studied (see, e.g., [6, 9–14]), where RF-powered nodes can harvest energy and receive information from the same RF signals concurrently. Among these works, stochastic geometry has been widely used for the performance characterization of simultaneous wireless information and energy transfer-enabled networks due to its tractability and capability of capturing the topological randomness and irregularity [12–14]. However, these works did not consider the cases where the energy transfer and information transmission links are separated, which is another interesting and important issue to be investigated in WPCNs [2]. Naturally, stochastic spatial models become the preferred choice (see, e.g., [3–5, 8, 15–17]). Recent related works can be

Na Deng is with the School of Information and Communication Engineering, Dalian University of Technology (DLUT), Dalian, 116024, China, and also with the National Mobile Communications Research Laboratory, Southeast University, Nanjing, 210096, China (e-mail: dengna@dlut.edu.cn). Martin Haenggi is with the Dept. of Electrical Engineering, University of Notre Dame, Notre Dame 46556, USA (e-mail: mhaenggi@nd.edu).

Part of this work has been presented at the 2019 IEEE International Conference on Communications (ICC'19) [1].

This work was supported by the National Natural Science Foundation of China under Grant 61701071, by the China Postdoctoral Science Foundation (2017M621129 and 2019T120204), by the open research fund of National Mobile Communications Research Laboratory, Southeast University (No. 2019D03), by the Fundamental Research Funds for the Central Universities (DUT19RC(4)014).

divided into two categories: (1) PPP-based analysis of WPCNs and (2) non PPP-based analysis of WPCNs.

PPP-Based Analysis of WPCNs: The authors of [3] studied the feasibility region of network parameters including node density and transmission power, under an outage constraint at the base station (BS), in an uplink cellular network solely powered by power beacons (PBs), where the locations of BSs and PBs were modeled as two independent PPPs and the users were uniformly distributed in the Voronoi cells formed by the BSs. A similar setup was considered in [4] with focus on secure D2D communications in a large-scale wirelessly powered cognitive cellular network. The authors of [5] investigated the transmission probability of D2D transmitters and the advantages of a cellular system with WET-enabled D2D communication over that with BSs alone in downlink transmission rate and the total energy cost, where the D2D transmitters were powered by RF signals from both BSs and PBs. In [8], we introduced the concept of the meta distribution to WPCNs and derived fine-grained performance metrics in terms of both the energy transfer and information transmission. In both [5] and [8], the RF power sources and the RF-powered nodes formed two independent PPPs. Researchers have also used the PPP model to investigate WET in heterogeneous cellular [18], relay [19], cognitive radio [20] and millimeter-wave networks [21]. Due to the independence between points in the PPP model, none of the aforementioned work considers the spatial correlations between RF power sources or RF-powered nodes, or the spatial correlation between the RF power sources and the RF-powered nodes. Assuming spatial independence, however, does not seem realistic considering the geographical factors and the specific WET policies (e.g., omni-directional or directed energy transfer).

Non PPP-Based Analysis of WPCNs: There have been a few works that focus on WPCNs in which the locations of either the RF-powered nodes or the RF power sources are modeled using a different point process than the PPP. For example, a repulsive point process named β-Ginibre point processes (β-GPP) [22] with the PPP as a special case was adopted in [15] to investigate the performance of wireless sensor networks with/without energy harvesting, where the spatial distributions of the RF-powered sensors and the RF energy sources follow two independent β-GPPs. In [16], the Poisson cluster process (PCP) was adopted to model the locations of backscatter transmitters in a wirelessly powered backscatter communication network. In particular, the backscatter nodes harvested energy from PBs located at the center of each cluster. Applying stochastic geometry, the coverage probability and transmission capacity were derived and optimized as functions of backscatter parameters. Similar to [16], the authors in [17] studied the uplink coverage and network throughput of a WPCN with users located around PBs, forming a truncated PCP with consideration of a practical transmission range. The works in [15–17], however, do not consider the spatial correlations between the RF power sources and the active RF-powered nodes that succeed in energy harvesting, i.e., the harvested energy correlation in the spatial domain, which circumvents some key analytical challenges that result from the high correlation between the locations of the active RF-powered nodes and the amount of energy they can harvest from all sources of RF energy. These challenges will be handled carefully in this paper, and accordingly, the communication performance of such a WPCN with energy correlation in a stochastic geometry framework will be studied in detail.

C. Contributions

In this paper, we investigate the energy correlation in wirelessly powered networks, i.e., the spatial correlation of active RF-powered nodes, which are those that harvest enough energy from the RF transmitters, or, equivalently, how likely a node at a particular location succeeds in harvesting energy when a nearby node succeeds. As discussed above, since so far such energy correlation has not been studied, we propose a new point process, named *energized point process* (EPP), as a model to capture the critical influence of the random field of harvested energy on the spatial distribution of active RF-powered nodes. The amount of energy that can be harvested strongly depends on the spatial configuration of the RF power sources and the energy harvesting model. We therefore concretize the EPP by focusing on the spatial correlation of the energy harvested from a Poisson field of RF power sources and considering two energy harvesting models with different degrees of practicality.

We start with a simple model dependent on the large-scale path loss alone, named path loss-based energy harvesting model (PLEHM), and then extend it to a practical one that includes more factors such as the random channel gains, random effects in the energy detection, and conversion efficiency at the receiver, named practical energy harvesting model (PEHM). Under the two models, we derive the first- and second-order statistics (density and pair correlation function) to characterize the spatial correlation of their corresponding EPPs. We establish that the EPPs under both models exhibit positive correlations, which means "attraction" exists between the locations of active RF-powered nodes. To show the effect of such spatial correlation caused by energy harvesting on the communication performance, we further use a fitted PCP to provide good approximations for the transmission success probability and the area spectral efficiency.

We also investigate the impacts of key parameters including the RF power source density λ_{p}, the energy threshold ξ, and the portion of energy transfer time η on the energy correlation as well as the communication performance. Our findings suggest that (1) the three parameters λ_{p}, ξ, η have strong effects on the spatial statistics of the EPP while the path loss exponent α does not; (2) comparing PLEHM with PEHM, the random factors in practical scenarios play a critical role in determining the energy harvesting success probability and hence the spatial characteristics of the energized RF-powered nodes; (3) Due to the neglect of the energy correlation, the conventional PPP-based results have significant deviations from the exact EPP-based analytical results and simulations, while the approximations provided by fitted PCPs are shown to be extremely accurate and (4) η and ξ are key parameters to balance the trade-off between the energy transfer and the information transmission phases. For all system parameters,

there is an optimal η or ξ achieving the maximal area spectral efficiency.

The proposed EPP model is attractive for many scenarios involving energy harvesting wireless communications such as wirelessly powered ad hoc networks, wirelessly powered cellular networks, and other IoT-inspired applications of the future.

D. Organization

The rest of the paper is organized as follows. In Section II, we introduce the EPP, two energy harvesting models and the communication model. Section III presents the analytical results for the energy harvesting phase, in particular, the first- and second-order statistics of the EPP. Section IV details the information transmission phase that covers the analysis of the transmission success probability and the area spectral efficiency. And Section V offers the concluding remarks.

II. System Model

We consider a wireless network powered solely by ambient RF transmitters (which may include dedicated power beacons, cellular base stations, WiFi hotspots, etc.), where the locations of RF transmitters and RF-powered nodes follow two point processes $\Phi_{\rm p}$ and $\Phi_{\rm d}$, respectively. We first formally define the EPP, which is formed by the RF-powered nodes that succeed in harvesting enough energy for subsequent transmission.

A. The Energized Point Process

Definition 1 (**Energized point process, EPP**). *Let $\Phi_{\rm p}$ and $\Phi_{\rm d}$ be two point processes. The energized point process $\Phi_{\rm e}$ is defined as*

$$\Phi_{\rm e} \triangleq \{x \in \Phi_{\rm d} \colon E(x, \Phi_{\rm p}) = 1\}, \tag{1}$$

where $E \in \{0, 1\}$ is the energy indicator function describing whether enough energy can be harvested from $\Phi_{\rm p}$ at location x.

In this paper, the two point processes $\Phi_{\rm p}$ and $\Phi_{\rm d}$ are assumed to be two independent homogeneous PPPs of densities $\lambda_{\rm p}$ and $\lambda_{\rm d}$, respectively. The resulting EPP is a dependent thinning of $\Phi_{\rm d}$ and can be viewed as a Cox process [7, Def. 3.3] with intensity field $\kappa(x) = \lambda_{\rm d} E(x, \Phi_{\rm p})$.

B. Path Loss-Based Energy Harvesting Model (PLEHM)

Since the amount of the harvested energy depends strongly on the locations of the nearby RF transmitters as well as the propagation loss experienced by the RF signals, we first consider a simplified energy harvesting model, where the signals from RF transmitters merely experience the large-scale path loss. Letting $\ell(x-y) \triangleq \|x-y\|^{-\alpha_{\rm p}}$ represent the path loss between transmitter x and receiver y with exponent $\alpha_{\rm p}$ for the energy transfer link, the harvested energy at x, which is the aggregated received signal strength from all the RF transmitters in $\Phi_{\rm p}$, is given by

$$\varepsilon(x, \Phi_{\rm p}) = \sum_{y \in \Phi_{\rm p}} \ell(y - x). \tag{2}$$

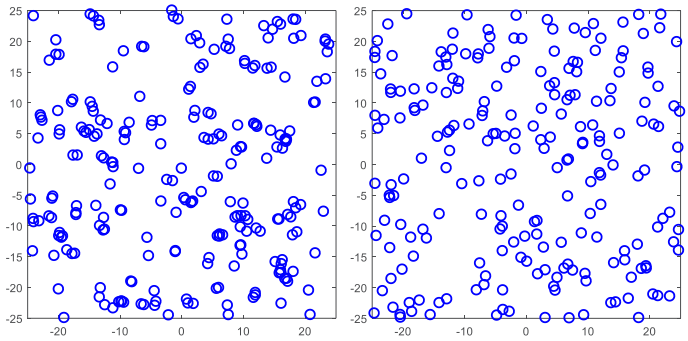

Fig. 1. Comparison of the EPP (left) and PPP (right). For the EPP, the PEHM is adopted with default parameter setting. For both point processes, the density is 0.0922.

C. Practical Energy Harvesting Model (PEHM)

Furthermore, we consider a practical energy harvesting model that includes more factors, such as channel gains, random effects in the energy detection and conversion at the receiver side as well as resource allocation for energy and information transfer phases. The channel (power) gain between transmitter x and receiver y is given by $h_{xy}\ell(x-y)$ where h_{xy} models the small-scale fading and $\ell(x-y)$ represents the large-scale path loss as in PLEHM. We assume that all fading coefficients are i.i.d. exponential (Rayleigh fading) with $\mathbb{E}(h_{xy}) = 1$. The transmit power of the RF transmitters is assumed to be one. Using the energy harvesting model in [23], the harvested energy $\varepsilon(x, \Phi_{\rm p})$ at the RF-powered node x can be quantified as

$$\varepsilon(x, \Phi_{\rm p}) = \frac{\nu\eta\rho}{1+F} \sum_{y \in \Phi_{\rm p}} h_{yx}\ell(y - x), \tag{3}$$

where the term $\frac{\nu}{1+F}$ captures the randomness[1] in the detection of the actual harvested energy, F follows an exponential distribution with parameter ζ, and ν is chosen so that $\frac{\nu}{1+F}$ has an expectation of 1, i.e., $\nu = \frac{1}{-\zeta e^{\zeta}\,\mathrm{Ei}(-\zeta)}$, where Ei is the exponential integral function defined by $\mathrm{Ei}(x) = -\int_{-x}^{\infty} e^{-t}/t\mathrm{d}t$. ρ is the efficiency of the conversion from RF to DC power and η is the fraction of a time slot allocated for energy harvesting.

Under both models, the energy indicator function is defined as

$$E(x, \Phi_{\rm p}) \triangleq \mathbf{1}(\varepsilon(x, \Phi_{\rm p}) > \xi), \tag{4}$$

where ξ is the energy threshold and $\mathbf{1}$ is the indicator function. This equation means an RF-powered node becomes active if and only if the amount of energy it can harvest exceeds the energy threshold. Note that (3) and (4) capture both linear and non-linear harvesting models. If the actual harvested energy is a non-linear function f of ε, where f is assumed strictly monotonically increasing, then ξ in (4) merely needs to be replaced by $f^{-1}(\xi)$ to capture the non-linearity. All the subsequent analysis and results remain the same.

Fig. 1 shows a comparison between the realizations of the PEHM-based EPP and PPP with the same density. It is

[1]This randomness can be understood as a random noise (e.g., electrical or in the channel) in the detection of the actual harvested energy [23].

TABLE I. Symbols and descriptions

Symbol	Description	Default value
$\Phi_{\rm p}$, $\lambda_{\rm p}$	RF transmitters PPP and density	$\rm N/A, 0.1$
$\Phi_{\rm d}$, $\lambda_{\rm d}$	RF-powered nodes PPP and density	$\rm N/A, 1$
$\Phi_{\rm e}$, $\lambda_{\rm e}$	Active RF-powered nodes EPP and density	$\rm N/A, N/A$
$\varepsilon(x, \Phi_{\rm p})$	The harvested energy at the RF-powered node x from RF transmitters $\Phi_{\rm p}$	$\rm N/A$
$\alpha_{\rm p}, \alpha_{\rm d}$	The path loss exponent of the energy/information link	4, 4
$p_{\rm e}, p_{\rm s}$	The success probability of the energy/information link	$\rm N/A, N/A$
$p_{\rm joint}(r)$	The joint success probability of energy harvesting	$\rm N/A$
$g_{\rm e}(r)$	The pair correlation function of the EPP	$\rm N/A$
ξ, θ, τ	The energy/SIR/spectrum efficiency threshold	1,1,1
η	The portion of time in the energy transfer phase	0.5
ρ	The efficiency of the conversion from RF to DC power	0.3 [23]
ζ	The parameter for random effect in energy harvesting	0.01 [23]
ν	The normalization factor for random effect in energy harvesting	$\rm N/A$
$r_{\rm d}$	The distance of information link between the transmitter-receiver pair	1
$\lambda_l, \sigma^2, \bar{c}$	The parameters of the fitted Thomas cluster process	$\rm N/A, N/A, N/A$

observed that the spatial distribution of the active RF-powered nodes exhibits significant clustering relative to the PPP.

D. Communication Model

We assume that RF-powered nodes adopt a time-switched "harvest-then-transmit" strategy in each time slot, and RF transmitters use frequencies outside the data band and hence cause no interference to the information transmission of RF-powered nodes. Specifically, in each time slot, each RF-powered node first uses a fraction η of the time slot to harvest energy from RF transmitters and then transmits the information to its corresponding receiver during the remaining fraction $1-\eta$ of time if the harvested energy satisfies the minimum requirement for signal transmission. Each RF-powered node is assumed to be battery-less and utilize the instantaneously harvested RF energy to supply its operation. It is also assumed that each RF-powered node has a dedicated receiver at distance $r_{\rm d}$ in a random orientation, i.e., the RF-powered nodes and their receivers form a Poisson bipolar network [7, Def. 5.8]. Hence, the active RF-powered nodes and their receivers form a Cox bipolar network. The transmit power of the RF-powered nodes is assumed to be one.

Table I summarizes the parameters of the network model with their descriptions, and default values are given where applicable.

III. Analytical Characterization of the EPP

In this section, we provide analytical results for the first- and second-order statistics to characterize the EPP. Since a translated and rotated version of $\Phi_{\rm e}$ can be obtained by translating and rotating $\Phi_{\rm p}$ and $\Phi_{\rm d}$, which are motion-invariant, $\Phi_{\rm e}$ is motion-invariant. As a result, the first-order statistic, i.e., the density $\lambda_{\rm e}$, is obtained by deriving the success probability $p_{\rm e}$ of the energy harvesting of the RF-powered node at the origin, i.e., $p_{\rm e} = \mathbb{P}(E(o, \Phi_{\rm p}) = 1)$ and $\lambda_{\rm e} = p_{\rm e}\lambda_{\rm d}$. For the second-order statistic, the pair correlation function (pcf) $g(x, y)$ [7, Def. 6.6] is usually used to describe the degree of correlation between two distinct points in the point process, and for a motion-invariant process, the pcf depends only on the distance $r = \|x - y\|$, i.e., $g(x, y) = g(r)$. The following lemma gives a general expression of the pcf for the EPP.

Lemma 1. *The pair correlation function of the EPP $\Phi_{\rm e}$ is*

$$g_{\rm e}(r) = \frac{p_{\rm joint}(r)}{p_{\rm e}^2}, \tag{5}$$

where $p_{\rm joint}(r) \triangleq \mathbb{P}(E(o, \Phi_{\rm p}) = 1, E(z_r, \Phi_{\rm p}) = 1)$ is the joint success probability that both the two points at locations $z_r = (r, 0)$ and o succeed in energy harvesting and thus are retained in $\Phi_{\rm e}$.

Proof: According to [7, Lemma 6.9], the pcf is given by

$$g(r) = \frac{1}{2\pi r}\frac{\rm d}{{\rm d}r}K(r), \tag{6}$$

where $K(r)$ is Ripley's K function [7, Def. 6.8], defined as

$$K(r) \triangleq \frac{1}{\lambda}\mathbb{E}_o^!\Phi\big(b(o, r)\big), \tag{7}$$

where $\mathbb{E}_o^!$ denotes the expectation with respect to the reduced Palm distribution of Φ given that $o \in \Phi$. We first calculate $\mathbb{E}_o^!\Phi_{\rm e}\big(b(o, r)\big)$, i.e., the mean number of extra points within distance r of the origin. A point of $\Phi_{\rm d}$ at location x with distance $u = \|x\|$ is retained in $\Phi_{\rm e}$ if $E(x, \Phi_{\rm p}) = 1$ under the condition that $E(o, \Phi_{\rm p}) = 1$ (because the point at the origin is already retained in $\Phi_{\rm e}$). And the motion-invariance of $\Phi_{\rm d}$ makes the condition of $E(x, \Phi_{\rm p}) = 1$ equivalent to that with $x = (u, 0)$. Since the density of the points in $\Phi_{\rm d}$ at distance u is $2\pi\lambda_{\rm d}u$, we have

$$\begin{aligned}
&\mathbb{E}_o^!\Phi_{\rm e}\big(b(o, r)\big) \\
&= 2\pi\lambda_{\rm d}\int_0^r \mathbb{P}(E((u, 0), \Phi_{\rm p}) = 1 \mid E(o, \Phi_{\rm p}) = 1)u{\rm d}u \\
&= \frac{2\pi\lambda_{\rm d}}{p_{\rm e}}\int_0^r \mathbb{P}(E((u, 0), \Phi_{\rm p}) = 1, E(o, \Phi_{\rm p}) = 1)u{\rm d}u.
\end{aligned} \tag{8}$$

The final result is obtained by substituting (8) and (7) into (6). ■

A. The PLEHM-based EPP

In this model, the harvested energy $\varepsilon(x,\Phi_{\rm p})$ at the RF-powered node x merely depends on the large-scale path loss. Unless otherwise stated, $\varepsilon(x,\Phi_{\rm p})$ is henceforth replaced by $\varepsilon(x)$ for the sake of brevity. To determine the first- and second-order statistics of the PLEHM-based EPP, we need to first derive the energy harvesting success probability of the RF-powered node at the origin, which can be obtained through the characteristic function method[2] and the Gil-Pelaez theorem [24]. For $\alpha_{\rm p}>2$, the characteristic function $\varphi_{\varepsilon(o)}(w)$ is given by [7, Sec. 5.15],

$$\varphi_{\varepsilon(o)}(w)=\exp\big(-\lambda_{\rm p}\pi\Gamma(1-\delta_{\rm p})w^{\delta_{\rm p}}e^{-j\pi\delta_{\rm p}/2}\big),\quad w\geq 0, \tag{9}$$

where $j\triangleq\sqrt{-1}$ and $\delta_{\rm p}\triangleq 2/\alpha_{\rm p}$. Using the Gil-Pelaez theorem [24], we have

$$\begin{aligned}p_{\rm e}&=\frac{1}{2}+\frac{1}{\pi}\int_0^\infty\frac{\Im\big(e^{-jw\xi}\varphi_{\varepsilon(o)}(w)\big)}{w}{\rm d}w\\&=\frac{1}{2}+\frac{1}{\pi}\int_0^\infty e^{-\lambda_{\rm p}\pi\Gamma(1-\delta_{\rm p})w^{\delta_{\rm p}}\cos(\delta_{\rm p}\pi/2)}\\&\quad\times\frac{\sin\big(\lambda_{\rm p}\pi\Gamma(1-\delta_{\rm p})w^{\delta_{\rm p}}\sin(\delta_{\rm p}\pi/2)-w\xi\big)}{w}{\rm d}w.\end{aligned} \tag{10}$$

Since $|\varphi_{\varepsilon(o)}(w)|$ essentially decreases exponentially with w, this integral can be evaluated very efficiently. For the special case $\alpha_{\rm p}=4$, we have

$$\varphi_{\varepsilon(o)}(w)=\exp\big(-\lambda_{\rm p}\pi^{3/2}\sqrt{w}e^{-j\pi/4}\big),\quad w\geq 0, \tag{11}$$

which is the characteristic function of a random variable with inverse gamma distribution. In this case, the energy harvesting success probability admits the closed-form expression

$$p_{\rm e}=1-\frac{1}{\sqrt{\pi}}\Gamma\Big(\frac{1}{2},\frac{\pi^3\lambda_{\rm p}^2}{4\xi}\Big). \tag{12}$$

Fig. 2 plots the density of the PLEHM-based EPP as a function of the energy threshold ξ for different path loss exponents $\alpha_{\rm p}$. It is observed that the density of the energized RF-powered nodes is increased when the path loss exponent is smaller. However, as ξ increases past the intersection point (at ξ slightly larger than 5 dB), the situation is reversed. This is because under a higher energy requirement, only those nodes located within the disks with radius of 1 centered at the RF power sources can succeed in energy harvesting. And in this case, the unbounded path loss model with the propagation distance smaller than 1 has an opposite effect of $\alpha_{\rm p}$. However, since the curves for $\xi>5$ dB are quite close to each other, the impact of the unbounded path loss model is negligible, and it has superior tractability.

The pcf under this model can be obtained by the following theorem. For notational convenience, we define $\psi(t,r,\theta)\triangleq\sqrt{t^2+r^2-2rt\cos\theta}$.

Theorem 1. *The joint success probability of two points within distance r for PLEHM is given by*

$$p_{\rm joint}(r)=p_{\rm e}-\frac{1}{4}\big(1-u(\xi)\big), \tag{13}$$

[2]The characteristic function of a random variable X is $\varphi_X(w)\triangleq\mathbb{E}(e^{jwX})$.

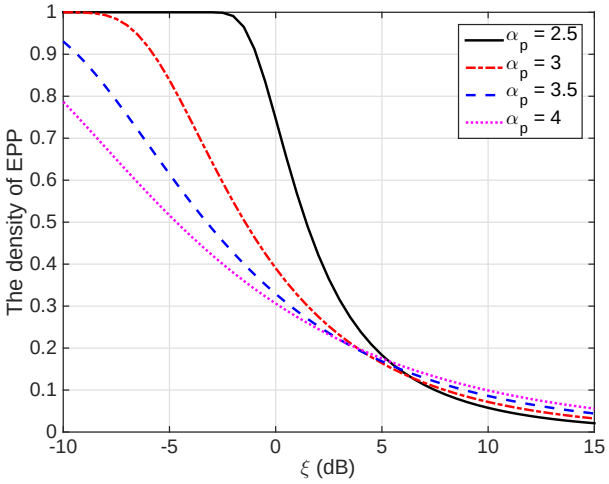

Fig. 2. The density of the PLEHM-based EPP versus ξ for different $\alpha_{\rm p}$ ($\lambda_{\rm d}=1$).

where

$$\begin{aligned}u(\xi)\triangleq-\frac{2}{\pi^2}\int_0^\infty\int_0^\infty\frac{1}{w_1w_2}\Re\Big[&\varphi(w_1,w_2)e^{-j\xi(w_1+w_2)}\\&-\varphi(w_1,-w_2)e^{-j\xi(w_1-w_2)}\Big]{\rm d}w_1{\rm d}w_2\end{aligned} \tag{14}$$

and

$$\varphi(w_1,w_2)\triangleq\exp\Big(\lambda_{\rm p}\int_0^\infty\int_0^{2\pi}(e^{jw_1t^{-\alpha_{\rm p}}+jw_2\psi(t,r,\theta)^{-\alpha_{\rm p}}}-1)t{\rm d}t{\rm d}\theta\Big). \tag{15}$$

Proof: The joint success probability is

$$\begin{aligned}p_{\rm joint}(r)&=1-\mathbb{P}(\varepsilon(o)\leq\xi)-\mathbb{P}(\varepsilon(z_r)\leq\xi)\\&\quad+\mathbb{P}(\varepsilon(o)\leq\xi,\varepsilon(z_r)\leq\xi)\\&\overset{(a)}{=}1-2\mathbb{P}(\varepsilon(o)\leq\xi)+\mathbb{P}(\varepsilon(o)\leq\xi,\varepsilon(z_r)\leq\xi),\end{aligned} \tag{16}$$

where step (a) follows since $\varepsilon(o)$ and $\varepsilon(z_r)$ are identically distributed (but dependent) random variables. The joint distribution of $\varepsilon(o)$ and $\varepsilon(z_r)$ is obtained by [25]

$$\mathbb{P}(\varepsilon(o)\leq\xi,\varepsilon(z_r)\leq\xi)=\frac{1}{4}\big(u(\xi)+4\mathbb{P}(\varepsilon(o)\leq\xi)-1\big), \tag{17}$$

where $u(\xi)$ is given in (14) and $\varphi(w_1,w_2)$ is the characteristic function of $\varepsilon(o)$ and $\varepsilon(z_r)$, given by

$$\varphi(w_1,w_2)\triangleq\mathbb{E}\big[\exp(jw_1\varepsilon(o)+jw_2\varepsilon(z_r))\big]. \tag{18}$$

To derive the $\varphi(w_1,w_2)$, we adopt a basic yet powerful technique described in [7, Sec. 5.15], and after several manipulations, we have the result in (15). Then, the final result can be obtained by substituting (17) into (16). ■

Since the exact expression of this joint success probability involves four nested integrals, it is difficult to calculate directly and efficiently, which motivates us to find an effective approximation to simplify the analytical result. For notational

convenience, we define $b(x,R)$ as the disk of radius R centered at x, let

$$V_r(R) \triangleq b(o,R) \cap b(z_r,R), \tilde{b}(z_r,R) = b(z_r,R) \setminus V_r(R), \tag{19}$$

and the intersection area of two disks of radius R at distance r is

$$A(R,r) = \begin{cases} 2R^2 \arccos\left(\frac{r}{2R}\right) - r\sqrt{R^2 - \frac{r^2}{4}} & \text{if } r \le 2R \\ 0 & \text{otherwise.} \end{cases} \tag{20}$$

The following corollary provides a simple approximation by decomposing the event of jointly succeeding in energy harvesting into several disjoint events.

Corollary 1. *Let $R_\xi \triangleq \xi^{-1/\alpha_\mathrm{p}}$ and $\beta_k \triangleq kN(N!)^{-1/N}/\xi$, where N is an integer that denotes the number of terms in the approximation. Then the joint probability of two points within distance r succeeding in energy harvesting for PLEHM can be approximated by*

$$p_{\mathrm{joint}}(r) \approx p_1(r) + 2p_2(r) + p_3(r), \tag{21}$$

where

$$p_1(r) = 1 - 2e^{-\lambda_\mathrm{p}\pi R^2} + e^{-\lambda_\mathrm{p}\left(2\pi R^2 - A(R_\xi,r)\right)},$$

$$p_2(r) = \frac{e^{-\lambda_\mathrm{p}\pi R_\xi^2} - e^{-\lambda_\mathrm{p}(2\pi R_\xi^2 - A(R_\xi,r))}}{\pi R_\xi^2 - A(R_\xi,r)} \sum_{k=0}^{N} (-1)^k \binom{N}{k} \times e^{-2\pi\lambda_\mathrm{p}\int_{R_\xi}^{\infty}(1-e^{-\beta_k t^{-\alpha_\mathrm{p}}})t\mathrm{d}t} \int\limits_{\tilde{b}(z_r,R_\xi)} e^{-\beta_k |x|^{-\alpha_\mathrm{p}}} \mathrm{d}x,$$

$$p_3(r) = e^{-\lambda_\mathrm{p}\left(2\pi R_\xi^2 - A(R_\xi,r)\right)} \sum_{k=0}^{N} (-1)^k \binom{N}{k} \times \exp\Big(- 2\pi\lambda_\mathrm{p} \int_{R_\xi}^{\infty} (1 - e^{-\beta_k t^{-\alpha_\mathrm{p}}}) t\mathrm{d}t \Big). \tag{22}$$

Moreover, the joint probability $p_{\mathrm{joint}}(r)$ in (21) becomes exact as $N \to \infty$.

Proof: See Appendix A.

Fig. 3 illustrates the pcfs of the PLEHM-based EPP for different path loss exponent α_p and energy threshold ξ, where $N = 20$ for calculating the approximation in Corollary 1, and, for comparison, the simulation curves are estimated through the built-in function **pcf** in the **R language**. From this figure, we can observe that the approximation in Corollary 1 is quite close to the simulation result with the benefit of reducing the complex four nested integrals in the exact result to two nested integrals. An important observation is that all the pcfs are larger than that in the PPP case and decrease with the increase of r, which demonstrates the clustering behavior of the active RF-powered nodes and shows that the correlation between two active RF-powered nodes is weaker with a longer inter-distance. Moreover, compared with α_p, ξ is a more critical parameter for determining the spatial correlation between two energized RF-powered nodes. The higher the energy requirement, the more obvious the clustering behavior.

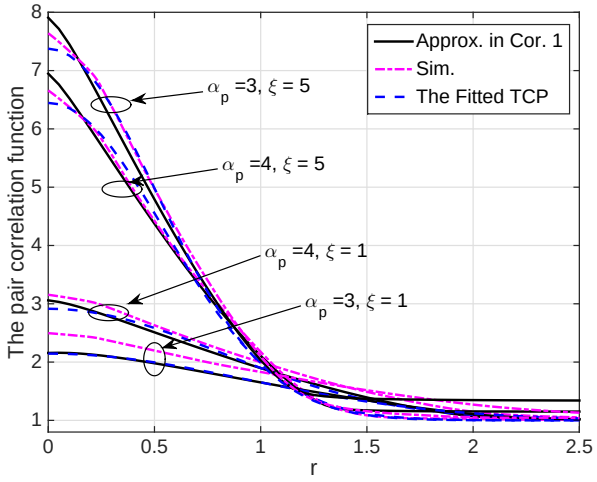

Fig. 3. The pcfs of the PLEHM-based EPP for different α_p and ξ ($N = 20$).

B. The PEHM-based EPP

Under this model, we first give an asymptotic upper bound on the density of the EPP, which is then proven to be very accurate with well controlled and mathematically quantified gaps.

Theorem 2. *Let $\bar{\xi} \triangleq \xi/(\zeta\nu\eta\rho)$ and*

$$\hat{p}_\mathrm{e} \triangleq 1 - \exp\Big(- \pi\lambda_\mathrm{p} \frac{\pi\delta_\mathrm{p}}{\sin(\pi\delta_\mathrm{p})} \bar{\xi}^{-\delta_\mathrm{p}} \Big). \tag{23}$$

The energy harvesting success probability for PEHM is upper bounded as $p_\mathrm{e} \le \hat{p}_\mathrm{e}$, and the density of the EPP follows $\lambda_\mathrm{e} \le \lambda_\mathrm{d}\hat{p}_\mathrm{e}$. Furthermore, $p_\mathrm{e} \lesssim \hat{p}_\mathrm{e}$ and $\lambda_\mathrm{e} \lesssim \lambda_\mathrm{d}\hat{p}_\mathrm{e}$, where '$\lesssim$' stands for an asymptotic upper bound, i.e., $\exists t > 0$ s.t. $p_\mathrm{e} < \hat{p}_\mathrm{e}$ and $\lambda_\mathrm{e} < \lambda_\mathrm{d}\hat{p}_\mathrm{e}$, $\forall \zeta < t$.

Proof: Letting $I_o \triangleq \sum_{y \in \Phi_\mathrm{p}} h_{yo}\ell(y)$, we have

$$\begin{aligned} p_\mathrm{e} &= \mathbb{P}\Big(\frac{\nu\eta\rho}{F+1} I_o \ge \xi\Big) \\ &\le \mathbb{P}\Big(F \le \frac{\nu\eta\rho}{\xi} I_o\Big) \\ &= 1 - \mathbb{E}\Big[\exp\Big(-I_o/\bar{\xi}\Big)\Big] \\ &\overset{(a)}{=} 1 - \exp\Big(- \pi\lambda_\mathrm{p} \frac{\pi\delta_\mathrm{p}}{\sin(\pi\delta_\mathrm{p})} \bar{\xi}^{-\delta_\mathrm{p}} \Big), \end{aligned} \tag{24}$$

where step (a) uses the Laplace transform of the interference in Poisson networks [7, Sec. 5.17]. Hence, the density λ_e of the EPP Φ_e is given by

$$\lambda_\mathrm{e} = \lambda_\mathrm{p} p_\mathrm{e} \le \lambda_\mathrm{p}\hat{p}_\mathrm{e}. \tag{25}$$

Next, we show the asymptotic property of the bound. Letting $Y = \nu\eta\rho I_o/\xi$, we have

$$\begin{aligned} p_\mathrm{e} - \hat{p}_\mathrm{e} &= \mathbb{P}(F \le Y - 1) - \mathbb{P}(F \le Y) \\ &= \mathbb{P}(F > Y) - \mathbb{P}(F > Y - 1) \\ &= \mathbb{E}_Y\Big[\big(e^{-\zeta Y} - e^{-\zeta(Y-1)}\big)\mathbf{1}_{Y \ge 1} + \big(e^{-\zeta Y} - 1\big)\mathbf{1}_{Y<1}\Big] \end{aligned}$$

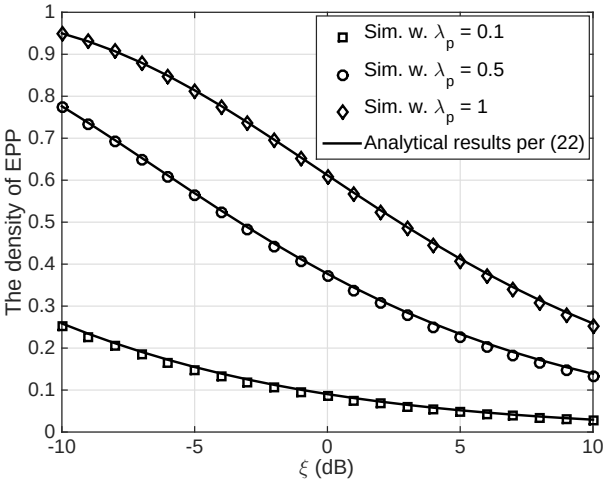

Fig. 4. The density of the PEHM-based EPP versus ξ for different $\lambda_{\rm p}$.

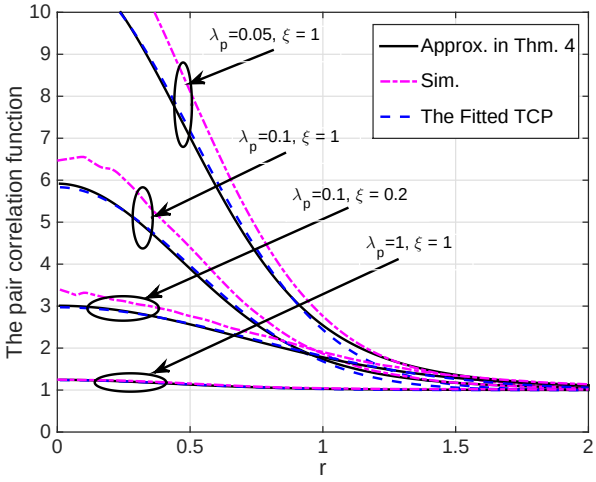

Fig. 5. The pcfs of the PEHM-based EPP with different $\lambda_{\rm p}$ and ξ.

$$\geq \mathbb{E}_Y\Big[\big(e^{-\zeta}-1\big)\mathbf{1}_{Y\geq 1}+\big(e^{-\zeta}-1\big)\mathbf{1}_{Y<1}\Big] = e^{-\zeta}-1. \tag{26}$$

Thus, for an arbitrary ζ, $p_{\rm e}$ is bounded by

$$\hat{p}_{\rm e}+e^{-\zeta}-1 \leq p_{\rm e} \leq \hat{p}_{\rm e}. \tag{27}$$

Since $p_{\rm e}\to\hat{p}_{\rm e}$ as $\zeta\to 0$, we have $p_{\rm e}\lesssim\hat{p}_{\rm e}$. ■

The following theorem provides analytical results for bounding the joint success probability and approximating the pcf of the EPP.

Theorem 3. *Let*

$$\hat{p}_{\rm joint}(r) \triangleq 1-2\exp\Big(-\pi\lambda_{\rm p}\frac{\pi\delta_{\rm p}}{\sin(\pi\delta_{\rm p})}\bar{\xi}^{-\delta_{\rm p}}\Big) + \exp\Big(-\lambda_{\rm p}\int_0^{\infty}\int_0^{2\pi}\chi(t,\theta)t{\rm d}t{\rm d}\theta\Big), \tag{28}$$

where

$$\chi(t,\theta)=1-\frac{1}{(1+\bar{\xi}^{-1}t^{-\alpha_{\rm p}})(1+\bar{\xi}^{-1}\psi(t,r,\theta)^{-\alpha_{\rm p}})}. \tag{29}$$

The joint success probability of two points within distance r for PEHM is asymptotically upper bounded as $p_{\rm joint}(r)\lesssim\hat{p}_{\rm joint}(r)$ and the corresponding pcf is approximated as $g_{\rm e}(r)\approx\hat{p}_{\rm joint}(r)/\hat{p}_{\rm e}^2$.

Proof: Letting $I_{z_r}\triangleq\sum_{y\in\Phi_{\rm p}}h_{yz_r}\ell(y-z_r)$, we have

$$\begin{aligned} p_{\rm joint}(r) &= \mathbb{P}(\varepsilon(z_r)>\xi,\varepsilon(o)>\xi)\\ &\leq \mathbb{P}\Big(F_o\leq\frac{\nu\eta\rho}{\xi}I_o, F_{z_r}\leq\frac{\nu\eta\rho}{\xi}I_{z_r}\Big)\\ &= \mathbb{E}\big[\big(1-e^{-I_o/\bar{\xi}}\big)\big(1-e^{-I_{z_r}/\bar{\xi}}\big)\big]\\ &= 1-2e^{-\pi\lambda_{\rm p}\frac{\pi\delta_{\rm p}}{\sin(\pi\delta_{\rm p})}\bar{\xi}^{-\delta_{\rm p}}}+\mathbb{E}\big[e^{-(I_o+I_{z_r})/\bar{\xi}}\big], \end{aligned} \tag{30}$$

where the PGFL of the PPP yields

$$\mathbb{E}\big[e^{-\bar{\xi}(I_o+I_{z_r})}\big] = \mathbb{E}\Big[\prod_{x\in\Phi_{\rm p}}\frac{1}{\big(1+\bar{\xi}^{-1}\ell(x)\big)\big(1+\bar{\xi}^{-1}\ell(x-z_r)\big)}\Big] = \exp\Big(-\lambda_{\rm p}\int_0^{\infty}\int_0^{2\pi}\chi(t,\theta)t{\rm d}t{\rm d}\theta\Big). \tag{31}$$

The asymptotic upper bound can be proved with a similar approach as in the proof of Thm. 2, and the pcf of the EPP is approximated through Lem. 1. ■

Fig. 4 shows the density of the PEHM-based EPP with the comparison between the analytical and simulation results. The analytical bounding result for the density is shown to provide an accurate approximation to the simulation result. In addition, the density of the EPP becomes smaller with the increase of ξ or the decrease of $\lambda_{\rm p}$.

Fig. 5 illustrates the pcfs of the PEHM-based EPP, where, similar to Fig. 3, the simulations are also estimated through the built-in function **pcf** in the **R language**. It shows that the analytical results in Thm. 3 provide a tight approximation; the small gap between the analytical and simulated curves vanishes as r increases, and also with increasing $\lambda_{\rm p}$. The slightly larger gap for small $\lambda_{\rm p}$ is a consequence of the fact that for small densities, it quickly becomes unlikely that a point of the EPP has a neighbor within distance r, which makes it harder to accurately estimate the pcf. Also, the **pcf** function in **R** is implemented according to the definition in (6), which includes a division by r and a derivative of the estimated $K(r)$ w.r.t. r, and these operations are not numerically robust at small r. Furthermore, we observe that all the pcfs are larger than in the PPP case, which again demonstrates the clustering behavior of the active RF-powered nodes and the correlation is monotonically decreasing with r. Moreover, a smaller $\lambda_{\rm p}$ or a larger ξ leads to a larger pcf for a fixed r, which means that the correlation between two active RF-powered nodes is stronger with a smaller $\lambda_{\rm p}$ or a larger ξ. This is because whether an RF-powered node succeeds in harvesting enough energy is chiefly determined by its nearby (especially the nearest) RF transmitters, and it is more likely for different RF-powered nodes to have the same nearby (nearest) RF transmitters in a

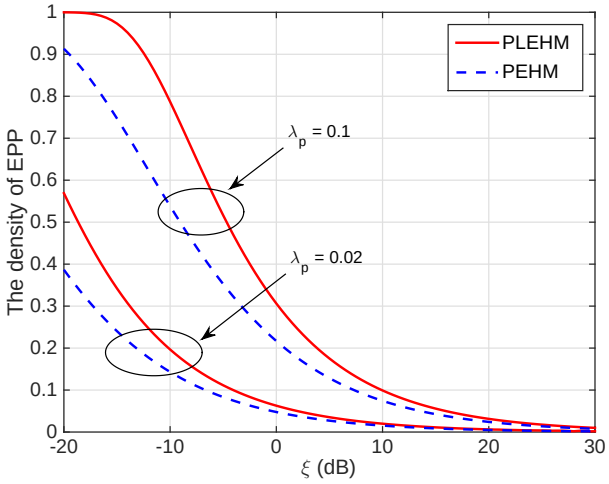

Fig. 6. The comparison of density for PLEHM- and PEHM-based EPPs with $\eta = \rho = 1$.

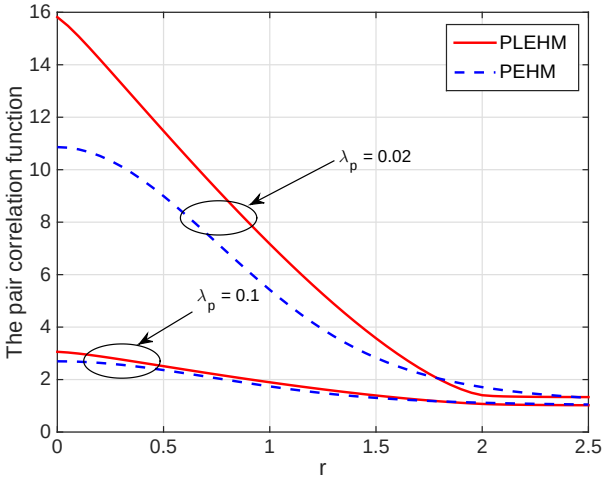

Fig. 7. The comparison of pcf for PLEHM- and PEHM-based EPPs with $\eta = \rho = 1$.

sparse deployment of RF transmitters.

C. Comparison Between PLEHM- and PEHM-based EPPs

An interesting question is what role the random factors (including small-scale fading and the randomness in the detection of the harvested energy) play in the spatial characteristics of the EPP, i.e., the random effects on the energy correlation. To answer this question, we compare the first- and second-order statistics of the PLEHM- and PEHM-based EPPs.

Fig. 6 gives the density as a function of ξ for the two EPPs. It can be seen that the randomness has a strong effect on the density of the EPP due to the introduction of uncertainties to the energy transfer link. According to the energy harvesting model in PEHM (Eq. (4) in Sec. II-C), there are mainly two random factors, i.e., the small-scale fading h_{xy} and the randomness in the detection $\frac{\nu}{1+F}$, where h_{xy} and F follow two exponential distributions with expectations of 1 and ζ. Since the probabilities of $h_{xy} < 1$ and $\frac{\nu}{1+F} < 1$ are about 0.632 and 0.79, respectively, the number of the nodes that harvest enough energy in PEHM is smaller than that in PLEHM.

Fig. 7 compares the pcfs between PLEHM and PEHM for different $\lambda_{\rm p}$. Different from the first-order statistic, the pcfs of the two models are quite close to each other when $\lambda_{\rm p} = 0.1$, which indicates that under a large density of RF power sources these random factors have little effect on the energy correlation since for a sufficiently large number of ambient RF power sources, the energy success probability is high enough so that the EPP in this case has weak energy correlation between two energized nodes. In contrast, when $\lambda_{\rm p}$ becomes small (e.g., $\lambda_{\rm p} = 0.02$), the energy correlation becomes stronger and the effect of randomness becomes more evident, especially for small r.

IV. Analysis of the Information Transmission Performance

For the information transmission phase, the properties of the desired signal and the interference strongly depend on the spatial distribution of the active RF-powered nodes, which determines the signal-to-interference ratio (SIR) and, in turn, the communication performance. Therefore, to fully investigate the effect of the energy correlation on the communication performance, in this section, we analyze the transmission success probability as well as the area spectral efficiency for both PLEHM and PEHM in an EPP-based wireless communication network.

A. Transmission Success Probability

The transmission success probability is defined as the complementary cumulative distribution function (ccdf) of the SIR, i.e., $P(\theta) \triangleq \mathbb{P}(\text{SIR} > \theta)$, where θ is the SIR threshold. Since the EPP is a stationary point process, we condition on the typical RF-powered node to be located at the origin, i.e. $o \in \Phi_{\rm e}$, and the corresponding typical receiver is at $z = (r_{\rm d}, 0)$. Letting $\Phi_{\rm e}^! = \Phi_{\rm e} \setminus \{o\}$ and $\ell(x-z) = \|x-z\|^{-\alpha_{\rm d}}$ for the information transmission link, the received signal-to-interference ratio (SIR) of the typical receiver is given by

$$\text{SIR} = \frac{\ell(r_{\rm d}) h_{oz}}{I(z)}, \tag{32}$$

where $I(z) = \sum_{x \in \Phi_{\rm e}^!} \ell(x-z) h_{xz}$. With signals subject to Rayleigh fading, the transmission success probability is the Laplace transform of $I(z)$ evaluated at $s = \theta r_{\rm d}^{\alpha_{\rm d}}$, given by

$$p_{\rm s}(\theta) = \mathcal{L}_{I(z)}\big(\theta r_{\rm d}^{\alpha_{\rm d}}\big), \tag{33}$$

and the Laplace transform of $I(z)$ is

$$\begin{aligned}\mathcal{L}_{I(z)}(s) &= \mathbb{E}\Big[\exp\Big(-s\sum_{x\in\Phi_{\rm e}^!}\ell(x-z)h_{xz}\Big)\Big] \\ &= \mathbb{E}_{\Phi_{\rm e}^!}\Big(\prod_{x\in\Phi_{\rm e}^!}\frac{1}{1+s\ell(x-z)}\Big) \\ &= \mathbb{E}_{o}^{!}\Big(\prod_{x\in\Phi_{\rm e}}\frac{1}{1+s\ell(x-z)}\Big),\end{aligned} \tag{34}$$

TABLE II. The parameter values of the fitted TCPs

PLEHM-based EPP					PEHM-based EPP				
$\alpha_{\rm p}$	3	4	3	4	$\lambda_{\rm p}$	0.05	0.1	0.1	1
ξ	1	1	5	5	ξ	1	0.2	1	1
$\lambda_{\rm l}$	0.1563	0.1258	0.0941	0.0998	$\lambda_{\rm l}$	0.0616	0.1437	0.1288	3.0022
σ^2	0.4446	0.3305	0.1327	0.1464	σ^2	0.1288	0.2807	0.1279	0.1116
$\bar{c}$	2.4970	2.4349	1.2493	1.4005	$\bar{c}$	0.7498	1.3270	0.7011	0.2038

where $\mathbb{E}_o^!$ denotes the expectation with respect to the reduced Palm distribution of the EPP, given that there is an active RF-powered node at the origin.

Due to the dependent thinning, an exact calculation of the success probability under the EPP model seems unfeasible. Thus, we resort to approximating the EPP with two common point processes, namely, the PPP and PCP, which have explicit PGFL expressions. The benefits of such approximations is to provide an accurate yet tractable analysis of the performance in the information transmission phase in wirelessly powered networks, which can hardly be obtained by either the PLEHM- or PEHM-based EPP directly.

- **PPP Approximation:** As a baseline model, we first approximate the EPP with a PPP using the first-order statistic $\lambda_{\rm e}$. From Slivnyak's theorem [7], conditioning on a point at the origin does not change the distribution of the rest of the process, and the reduced Palm distribution is the same as the distribution of the original PPP. Hence, $\mathcal{L}_{I(z)}(s)$ is approximated by

$$\mathcal{L}_{I_{\rm PPP}}(s) = \exp\Big(-\lambda_{\rm e} \int_{\mathbb{R}^2} \frac{1}{1+s^{-1}\ell^{-1}(x)} {\rm d}x \Big). \quad (35)$$

  When $\ell(x) = \|x\|^{-\alpha_{\rm d}}$, the Laplace transform can be simplified as

$$\mathcal{L}_{I_{\rm PPP}}(s) = \exp\Big(-\lambda_{\rm e}\pi \frac{\pi\delta_{\rm d}}{\sin(\pi\delta_{\rm d})} s^{\delta_{\rm d}} \Big), \quad (36)$$

  and the success probability is approximated as

$$p_{\rm s}(\theta) \approx \exp\Big(-\lambda_{\rm e} \frac{\pi^2\delta_{\rm d}}{\sin(\pi\delta_{\rm d})} r_{\rm d}^2 \theta^{\delta_{\rm d}} \Big). \quad (37)$$

- **PCP Approximation:** From the above discussion, the points in the EPP are clustered. The PCP also exhibits clustering and, in addition, leads to tractable results. Thus we provide another approximation of the EPP with a fitted PCP, namely the Thomas cluster process (TCP) [7, Def. 3.5], through matching the first- and second-order statistics.

  The first-order statistic matching yields

$$\lambda_{\rm e} = \lambda_l \bar{c}, \quad (38)$$

  where λ_l is the density of parent points of the cluster process and $\bar{c}$ is the average number of points in a cluster. For the TCP with variance σ^2, the pcf is [7, Section 6.4]

$$g_{\rm T}(r) = 1 + \frac{1}{4\pi\lambda_l\sigma^2} \exp\left(-\frac{r^2}{4\sigma^2} \right), \quad (39)$$

  where λ_l and σ are obtained using curve-fitting and $\bar{c}$ is then determined using (38). By using the **fmincon** function (minimizing the constrained nonlinear multivariable function) in **Matlab**, we fit the pcf of the TCP to the approximative analytical pcf of the EPP for different ζ and $\lambda_{\rm p}$. The fitting parameters of the TCP for PLEHM- and PEHM-based EPP are listed in Tables II, Fig. 3 and 5 also illustrate the fitted pcf curves of the TCP. The results show that the EPP can be closely approximated by the TCP.

  Through the fitted TCP, $I(z)$ can be approximated by the interference in Poisson cluster networks. According to [26, Eq .(34)], the Laplace transform of the interference is

$$\mathcal{L}_{I_{\rm PCP}}(s) = \exp\left\{ -\lambda_l \int_{\mathbb{R}^2} \big[1 - \exp(-\bar{c}\nu(s,y,z))\big] {\rm d}y \right\} \times \int_{\mathbb{R}^2} \exp(-\bar{c}\nu(s,y,z)) f(y) {\rm d}y, \quad (40)$$

  where

$$\nu(s,y,z) = \int_{\mathbb{R}^2} \frac{f(x)}{1+(s\ell(x-y-z))^{-1}} {\rm d}x, \quad (41)$$

  and $f(x)$ is the probability density function of the node distribution around the parent point. For the TCP, we have

$$f(x) = \frac{1}{2\pi\sigma^2} \exp\left(-\frac{\|x\|^2}{2\sigma^2} \right). \quad (42)$$

  Substituting (40) into (33), the success probability is approximated as $p_{\rm s}(\theta) \approx \mathcal{L}_{I_{\rm PCP}}(\theta r_{\rm d}^{\alpha_{\rm d}})$.

Fig. 8 illustrates the success probabilities with PPP and PCP approximations for PLEHM- and PEHM-based EPPs with different energy threshold ξ. From the figure, we can observe that the success probability improves as ξ increases, because the higher the energy threshold, the smaller the number of active RF-powered nodes, and thus the less interference suffered by the receiver. More importantly, the results show that the EPP-based transmission success probability, either the PLEHM-based EPP shown in Fig. 8(a) or the PEHM-based EPP shown in Fig. 8(b), can be approximated by the TCP-based results extremely well while the results in the PPP case are overly optimistic. The reason lies in the higher-order statistics of the EPP, which govern the interaction between nodes and strongly affect the success probability of the information transmission. Therefore, compared with the PPP, the PCP is a more suitable model for capturing the actual topology of the energized nodes, due to the positive energy correlation.

B. Area Spectral Efficiency

In addition to the transmission reliability (i.e., the success probability), which is a link-level performance, it is necessary to investigate the area spectral efficiency which is another

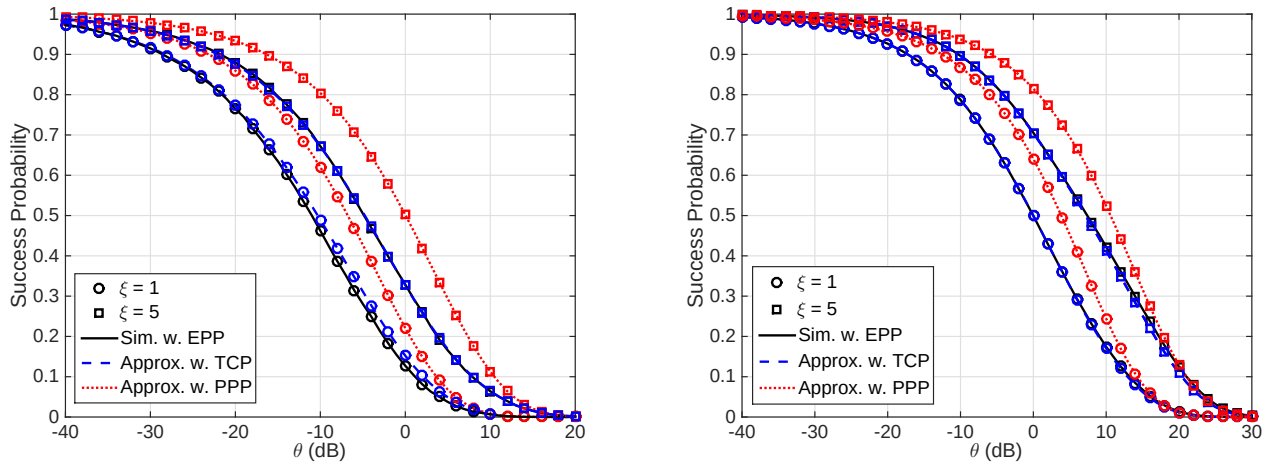

(a) PLEHM-based EPP (b) PEHM-based EPP

Fig. 8. The success probability with PPP and PCP approximations to the EPP.

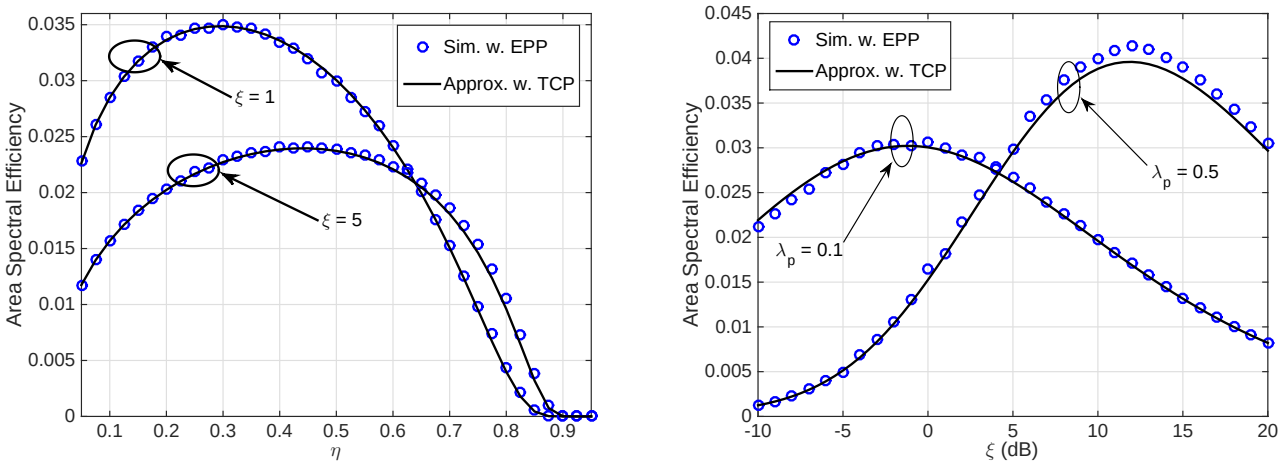

(a) Area spectral efficiency vs. η (b) Area spectral efficiency vs. ξ

Fig. 9. The area spectral efficiency for the PEHM-based EPP.

fundamental performance metric to characterize the network-level transmission effectiveness. Under fixed-rate transmission, the area spectral efficiency is expressed as

$$\begin{aligned} S(\tau) &= \lambda_{\mathrm{e}} p_{\mathrm{s}}(\theta)\tau \\ &= \lambda_{\mathrm{d}} p_{\mathrm{e}}(\xi) p_{\mathrm{s}}(2^{\tau/(1-\eta)} - 1)\tau, \end{aligned} \tag{43}$$

where $\tau \triangleq (1-\eta)\log_2(1+\theta)$ denotes the required spectrum efficiency of the RF-powered nodes. Since the energy harvesting success probability p_{e} increases with η while the success probability p_{s} of the information transmission decreases with η, the area spectral efficiency is expected to capture the trade-off between the energy transfer and the information transmission phases.

Fig. 9 explores the behavior of $S(\tau)$ as a function of η and ξ for different ξ and λ_{p}, respectively. It is observed that the approximations of the fitted TCP match the simulation results of the EPP very well, which again demonstrates the clustering behavior induced by the energy correlation.

In Fig. 9(a), for each value of ξ, there is an optimal η achieving the maximal area spectral efficiency. It is interesting to observe that there is an intersection point η_{i} between the two curves: when $\eta < \eta_{\mathrm{i}}$, the area spectral efficiency of $\xi = 1$ is significantly higher than that of $\xi = 5$ since the density of the EPP in the former case is higher than the latter case; while when $\eta > \eta_{\mathrm{i}}$, the result is just the opposite because in this case the densities of $\xi = 1, 5$ are almost the same but the EPP under $\xi = 5$ would cause stronger interference due to its stronger clustering than that under $\xi = 1$. This observation indicates that there is an important trade-off between the energy success probability and the information success probability and ξ is a key parameter that determines the density and the clustering degree of the EPP.

Similar to Fig. 9(a), for the given system parameters, there is always an optimal ξ achieving the maximal area spectral

efficiency, shown in Fig. 9(b). In addition, the optimal value of ξ increases with the density of the RF transmitters $\lambda_{\rm p}$. As ξ increases, the energy harvesting success probability and thus the density $\lambda_{\rm e}$ of active RF-powered nodes decrease, leading to an increase of the information transmission success probability $p_{\rm s}$. However, since the area spectral efficiency is determined by $\lambda_{\rm e}$ and $p_{\rm s}$ simultaneously, this figure also illustrates the key trade-off between the density of active RF-powered nodes (resulting from the energy harvesting success probability) and the information transmission success probability in terms of another key parameter, ξ.

V. Conclusions

Since the locations of the RF-power sources are a common source of randomness, the harvested energy is naturally correlated at nearby RF-powered node locations. To fully explore the energy correlation, a new point process, named EPP, is introduced as a model for the RF-powered nodes that successfully harvest enough energy. Under the assumption of Poisson distributed RF power sources and the two energy harvesting models, i.e., PLEHM and PEHM, we derived the first- and second-order statistics of the PLEHM- and PEHM-based EPPs. The key insight is that the EPP exhibits clustering, in other words, the energy harvested at nearby RF-powered nodes are positively correlated, which makes the interference in the communication phase stronger than in the mutually independent case.

Using the EPP to model the active RF-powered nodes, the information transmission success probability and the area spectral efficiency were investigated. Moreover, an approximation by a fitted TCP turns out to be matching the exact EPP-based result extremely accurately, while the PPP-based approximation, in contrast, has an obvious deviation. Among the system parameters, the energy threshold and the portion of the energy transfer time are the most influential parameters that have strong effects on the spatial correlation of the energized RF-powered nodes as well as the energy and information transmission performance, which should be set judiciously. Overall, both the analysis and approximation show that "attraction" exists between the energized node locations, and the widely used PPP-based model as well as the results derived from it deviate significantly from the exact ones.

Appendix A
Proof of Corollary 1

Proof: In PLEHM, the energy indicator is given by

$$E(x,\Phi_{\rm p})=\mathbf{1}(\sum_{y\in\Phi_{\rm p}}\ell(y-x)>\xi). \tag{44}$$

Thus a node necessarily succeeds in harvesting enough energy if there is at least one RF transmitter within a distance R_ξ. The event that two nodes jointly succeed in energy harvesting can be partitioned into the following four disjoint events according to whether these two nodes have a nearby RF transmitter within a distance R_ξ, given by

$$\Big\{\varepsilon(o)>\xi,\varepsilon(z_r)>\xi\Big\}=\bigcup_{i=1}^{4}\mathcal{A}_i, \tag{45}$$

where

$$\begin{aligned}
\mathcal{A}_1=&\Big\{\Phi_{\rm p}\big(b(o,R_\xi)\big)>0,\Phi_{\rm p}\big(b(z_r,R_\xi)\big)>0\Big\},\\
\mathcal{A}_2=&\Big\{\Phi_{\rm p}\big(b(o,R_\xi)\big)=0,\Phi_{\rm p}\big(b(z_r,R_\xi)\setminus V_r(R_\xi)\big)>0\Big\}\\
&\cap\Big\{\varepsilon(o)>\xi\Big\},\\
\mathcal{A}_3=&\Big\{\Phi_{\rm p}\big(b(o,R_\xi)\setminus V_r(R_\xi)\big)>0,\Phi_{\rm p}\big(b(z_r,R_\xi)\big)=0\Big\}\\
&\cap\Big\{\varepsilon(z_r)>\xi\Big\},\\
\mathcal{A}_4=&\Big\{\Phi_{\rm p}\big(b(o,R_\xi)\cup b(z_r,R_\xi)\big)=0,\varepsilon(o)>\xi,\varepsilon(z_r)>\xi\Big\}.
\end{aligned}$$

For event $\mathcal{A}_1$, it is partitioned into two disjoint events: one is that at least one RF transmitter falls in $V_r(R_\xi)$; the other is that at least one RF transmitter respectively falls in $b(o,R_\xi)\setminus V_r(R_\xi)$ and $b(z_r,R_\xi)\setminus V_r(R_\xi)$, conditioning on that no RF transmitter falls in $V_r(R_\xi)$. According to the total probability law, we have

$$\begin{aligned}
\mathbb{P}(\mathcal{A}_1)=&1-e^{-\lambda_{\rm p}A(R_\xi,r)}\\
&+e^{-\lambda_{\rm p}A_R(r)}\Big(1-e^{-\lambda_{\rm p}(\pi R^2-A(R_\xi,r))}\Big)^2\\
=&1-2e^{-\lambda_{\rm p}\pi R^2}+e^{-\lambda_{\rm p}\left(2\pi R^2-A(R_\xi,r)\right)}.
\end{aligned}\tag{46}$$

For event $\mathcal{A}_2$ and $\mathcal{A}_3$, due to the symmetry of o and z_r, we have $\mathbb{P}(\mathcal{A}_2)=\mathbb{P}(\mathcal{A}_3)$. Letting

$$\tilde{\mathcal{A}}_2=\Big\{\Phi_{\rm p}\big(b(o,R_\xi)\big)=0,\Phi_{\rm p}\big(b(z_r,R_\xi)\setminus V_r(R_\xi)\big)>0\Big\}, \tag{47}$$

the corresponding probability is

$$\begin{aligned}
\mathbb{P}(\mathcal{A}_2)=&\mathbb{P}(\tilde{\mathcal{A}}_2)\mathbb{P}(\mathcal{A}_2\mid\tilde{\mathcal{A}}_2)\\
=&\underbrace{e^{-\lambda_{\rm p}\pi R_\xi^2}\Big(1-e^{-\lambda_{\rm p}(\pi R_\xi^2-A(R_\xi,r))}\Big)}_{\mathbb{P}(\tilde{\mathcal{A}}_2)}\\
&\times\mathbb{P}\Big(\ell(x_0)+\Sigma_{x\in\tilde{\Phi}_{\rm p}(R_\xi)}\ell(x)>\xi\Big),
\end{aligned}\tag{48}$$

where $\tilde{\Phi}_{\rm p}(R_\xi)=\Phi_{\rm p}\setminus b(o,R_\xi)$, and x_0 is an RF transmitter uniformly and randomly distributed in the region $\tilde{b}(z_r,R_\xi)=b(z_r,R_\xi)\setminus V_r(R_\xi)$. Letting $\tilde{\varepsilon}=\Sigma_{x\in\tilde{\Phi}_{\rm p}(R_\xi)}\ell(x)$ and $\widetilde{\gamma}(n,x)=\gamma(n,x)/\Gamma(n)$, we have

$$\begin{aligned}
\mathbb{P}\Big(\ell(x_0)+\tilde{\varepsilon}>\xi\Big)\overset{(a)}{=}&\lim_{N\to\infty}\mathbb{P}\Big(U<\frac{\ell(x_0)+\tilde{\varepsilon}}{\xi}\Big)\\
=&\lim_{N\to\infty}\mathbb{E}\widetilde{\gamma}\Big(N,\frac{N\ell(x_0)+\tilde{\varepsilon}}{\xi}\Big)\\
\overset{(b)}{\approx}&\mathbb{E}\Big[\Big(1-e^{-\beta\frac{\ell(x_0)+\tilde{\varepsilon}}{\xi}}\Big)^N\Big]\\
=&\sum_{k=0}^{N}(-1)^k\binom{N}{k}\mathbb{E}\Big[e^{-\beta k\frac{\ell(x_0)+\tilde{\varepsilon}}{\xi}}\Big],
\end{aligned}\tag{49}$$

where step (a) introduces a dummy gamma distributed random variable $U\sim\mathrm{Gamma}(N,1/N)$ that converges to 1 as $N\to\infty$, and step (b) yields an approximation by using the finite N and the tight upper bound of the incomplete gamma function in [27] with $\beta=N(N!)^{-1/N}$. To evaluate the expectation in (49), by substituting $\beta_k=\beta k/\xi$, we have

$$\mathbb{E}\Big[e^{-\beta_k\left(\ell(x_0)+\tilde{\varepsilon}\right)}\Big]$$

$$= \mathbb{E}\Big[e^{-\beta_k \ell(x_0)}\Big]\mathbb{E}\Big[e^{-\beta_k \tilde{\varepsilon}}\Big]$$
$$= \mathbb{E}\Big[e^{-\beta_k \ell(x_0)}\Big]\mathbb{E}\Big[\prod_{x\in\tilde{\Phi}_{\rm p}(R_\xi)} e^{-\beta_k |x|^{-\alpha_{\rm p}}}\Big]$$
$$= \frac{\int_{\tilde{b}(z_r,R_\xi)} e^{-\beta_k |x|^{-\alpha_{\rm p}}} {\rm d}x}{\pi R_\xi^2 - A(R_\xi, r)} \times \exp\Big(-2\pi\lambda_{\rm p}\int_{R_\xi}^{\infty}(1-e^{-\beta_k t^{-\alpha_{\rm p}}})t{\rm d}t\Big). \quad (50)$$

For event $\mathcal{A}_4$, letting $\tilde{\mathcal{A}}_4 = \Big\{\Phi_{\rm p}\big(b(o,R_\xi)\cup b(z_r,R_\xi)\big)=0\Big\}$, we have

$$\mathbb{P}(\mathcal{A}_4) = \mathbb{P}\big(\tilde{\mathcal{A}}_4\big)\mathbb{P}\big(\varepsilon(o)>\xi, \varepsilon(z_r)>\xi \mid \tilde{\mathcal{A}}_4\big)$$
$$< \mathbb{P}\big(\tilde{\mathcal{A}}_4\big)\mathbb{P}\big(\varepsilon(o)>\xi \mid \tilde{\mathcal{A}}_4\big)$$
$$< e^{-\lambda_{\rm p}\left(2\pi R_\xi^2 - A(R_\xi,r)\right)}\mathbb{P}\Big(\Sigma_{x\in\tilde{\Phi}_{\rm p}(R_\xi)}\ell(x)>\xi\Big). \quad (51)$$

Using the same approach as in (49), we obtain

$$\mathbb{P}\Big(\Sigma_{x\in\tilde{\Phi}_{\rm p}(R_\xi)}\ell(x)>\xi\Big) \approx \sum_{k=0}^{N}(-1)^k\binom{N}{k} \times \exp\Big(-2\pi\lambda_{\rm p}\int_{R_\xi}^{\infty}(1-e^{-\beta_k t^{-\alpha_{\rm p}}})t{\rm d}t\Big). \quad (52)$$

■

REFERENCES

[1] N. Deng and M. Haenggi, "Energy correlation in wirelessly powered networks," in *IEEE International Conference on Communications (ICC'19)*, Shanghai, China, May 2019.

[2] S. Bi, C. K. Ho, and R. Zhang, "Wireless powered communication: opportunities and challenges," *IEEE Communications Magazine*, vol. 53, no. 4, pp. 117–125, Apr. 2015.

[3] K. Huang and V. K. N. Lau, "Enabling wireless power transfer in cellular networks: Architecture, modeling and deployment," *IEEE Transactions on Wireless Communications*, vol. 13, no. 2, pp. 902–912, Feb. 2014.

[4] Y. Liu, L. Wang, S. A. R. Zaidi *et al.*, "Secure D2D communication in large-scale cognitive cellular networks: A wireless power transfer model," *IEEE Transactions on Communications*, vol. 64, no. 1, pp. 329–342, Jan. 2016.

[5] L. Shi, L. Zhao, K. Liang, and H. Chen, "Wireless energy transfer enabled D2D in underlaying cellular networks," *IEEE Transactions on Vehicular Technology*, vol. 67, no. 2, pp. 1845–1849, Feb. 2018.

[6] S. Akbar, Y. Deng, A. Nallanathan *et al.*, "Simultaneous wireless information and power transfer in K-tier heterogeneous cellular networks," *IEEE Transactions on Wireless Communications*, vol. 15, no. 8, pp. 5804–5818, Aug. 2016.

[7] M. Haenggi, *Stochastic geometry for wireless networks*. Cambridge University Press, 2012.

[8] N. Deng and M. Haenggi, "The energy and rate meta distributions in wirelessly powered D2D networks," *IEEE Journal on Selected Areas in Communications*, vol. 37, no. 2, pp. 269–282, Feb. 2019.

[9] T. D. Ponnimbaduge Perera, D. N. K. Jayakody, S. K. Sharma *et al.*, "Simultaneous wireless information and power transfer (SWIPT): Recent advances and future challenges," *IEEE Communications Surveys & Tutorials*, vol. 20, no. 1, pp. 264–302, First quarter 2018.

[10] Z. Na, Y. Wang, X. Li *et al.*, "Subcarrier allocation based simultaneous wireless information and power transfer algorithm in 5G cooperative OFDM communication systems," *Physical Communication*, vol. 29, pp. 164–170, Aug. 2018.

[11] Z. Na, J. Lv, M. Zhang *et al.*, "GFDM based wireless powered communication for cooperative relay system," *IEEE Access*, vol. 7, pp. 50 971–50 979, 2019.

[12] O. Georgiou, "Simultaneous wireless information and power transfer in cellular networks with directional antennas," *IEEE Communications Letters*, vol. 21, no. 4, pp. 885–888, Apr. 2017.

[13] M. Di Renzo and W. Lu, "System-level analysis and optimization of cellular networks with simultaneous wireless information and power transfer: Stochastic geometry modeling," *IEEE Transactions on Vehicular Technology*, vol. 66, no. 3, pp. 2251–2275, Mar. 2017.

[14] A. I. Akin, I. Stupia, and L. Vandendorpe, "On the effect of blockage objects in dense MIMO SWIPT networks," *IEEE Transactions on Communications*, vol. 67, no. 2, pp. 1059–1069, Feb. 2019.

[15] H. Kong, P. Wang, D. Niyato, and Y. Cheng, "Modeling and analysis of wireless sensor networks with/without energy harvesting using Ginibre point processes," *IEEE Transactions on Wireless Communications*, vol. 16, no. 6, pp. 3700–3713, Jun. 2017.

[16] K. Han and K. Huang, "Wirelessly powered backscatter communication networks: Modeling, coverage, and capacity," *IEEE Transactions on Wireless Communications*, vol. 16, no. 4, pp. 2548–2561, Apr. 2017.

[17] L. Chen, W. Wang, and C. Zhang, "Stochastic wireless powered communication networks with truncated cluster point process," *IEEE Transactions on Vehicular Technology*, vol. 66, no. 12, pp. 11 286–11 294, Dec. 2017.

[18] A. H. Sakr and E. Hossain, "Analysis of K-tier uplink cellular networks with ambient RF energy harvesting," *IEEE Journal on Selected Areas in Communications*, vol. 33, no. 10, pp. 2226–2238, Oct. 2015.

[19] I. Krikidis, "Simultaneous information and energy transfer in large-scale networks with/without relaying," *IEEE Transactions on Communications*, vol. 62, no. 3, pp. 900–912, Mar. 2014.

[20] S. Lee, R. Zhang, and K. Huang, "Opportunistic wireless energy harvesting in cognitive radio networks," *IEEE Transactions on Wireless Communications*, vol. 12, no. 9, pp. 4788–4799, Sept. 2013.

[21] C. Psomas and I. Krikidis, "Energy beamforming in wireless powered mmWave sensor networks," *IEEE Journal on Selected Areas in Communications*, vol. 37, no. 2, pp. 424–438, Feb. 2019.

[22] N. Deng, W. Zhou, and M. Haenggi, "The Ginibre point process as a model for wireless networks with repulsion," *IEEE Transactions on Wireless Communications*, vol. 14, no. 1, pp. 107–121, Jan. 2015.

[23] X. Lu, I. Flint, D. Niyato *et al.*, "Self-sustainable communications with RF energy harvesting: Ginibre point process modeling and analysis," *IEEE Journal on Selected Areas in Communications*, vol. 34, no. 5, pp. 1518–1535, May 2016.

[24] J. Gil-Pelaez, "Note on the inversion theorem," *Biometrika*, vol. 38, pp. 481–482, Dec. 1951.

[25] N. Shephard and N. G. Shephard, "From characteristic function to distribution function: A simple framework for the theory," *Econometric Theory*, vol. 7, no. 4, pp. 519–529, 1991.

[26] R. Ganti and M. Haenggi, "Interference and outage in clustered wireless ad hoc networks," *IEEE Transactions on Information Theory*, vol. 55, no. 9, pp. 4067–4086, Sept. 2009.

[27] H. Alzer, "On some inequalities for the incomplete gamma function," *Mathematics of Computation*, vol. 66, no. 66, pp. 771–778, 1997.

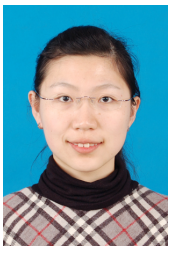

Na Deng (S'12-M'17) received the Ph.D. and B.S. degrees in information and communication engineering from the University of Science and Technology of China (USTC), Hefei, China, in 2015 and 2010, respectively. Currently she is an Associate Professor at Dalian University of Technology, Dalian, China. In 2013-2014, she was a Visiting Student in Prof. Martin Haenggi's group at the University of Notre Dame, Notre Dame, IN, USA, and in 2015-2016 she was a Senior Engineer at Huawei Technologies Co., Ltd., Shanghai, China. Her scientific interests include networking and wireless communications, green communications, and network design based on wireless big data.

Martin Haenggi (S'95-M'99-SM'04-F'14) received the Dipl.-Ing. (M.Sc.) and Dr.sc.techn. (Ph.D.) degrees in electrical engineering from the Swiss Federal Institute of Technology in Zurich (ETH) in 1995 and 1999, respectively. Currently he is the Freimann Professor of Electrical Engineering and a Concurrent Professor of Applied and Computational Mathematics and Statistics at the University of Notre Dame, Indiana, USA. In 2007-2008, he was a visiting professor at the University of California at San Diego, and in 2014-2015 he was an Invited Professor at EPFL, Switzerland. He is a co-author of the monographs "Interference in Large Wireless Network" (NOW Publishers, 2009) and "Stochastic Geometry Analysis of Cellular Networks" (Cambridge University Press, 2018) and the author of the textbook "Stochastic Geometry for Wireless Networks" (Cambridge, 2012), and he published 15 single-author journal articles. His scientific interests lie in networking and wireless communications, with an emphasis on cellular, amorphous, ad hoc (including D2D and M2M), cognitive, and vehicular networks. He served as an Associate Editor of the Elsevier Journal of Ad Hoc Networks, the IEEE Transactions on Mobile Computing (TMC), the ACM Transactions on Sensor Networks, as a Guest Editor for the IEEE Journal on Selected Areas in Communications, the IEEE Transactions on Vehicular Technology, and the EURASIP Journal on Wireless Communications and Networking, as a Steering Committee member of the TMC, and as the Chair of the Executive Editorial Committee of the IEEE Transactions on Wireless Communications (TWC). From 2017 to 2018, he was the Editor-in-Chief of the TWC. Currently he is an editor for MDPI Information. For both his M.Sc. and Ph.D. theses, he was awarded the ETH medal. He also received a CAREER award from the U.S. National Science Foundation in 2005 and three awards from the IEEE Communications Society, the 2010 Best Tutorial Paper award, the 2017 Stephen O. Rice Prize paper award, and the 2017 Best Survey paper award, and he is a Clarivate Analytics Highly Cited Researcher.